NJC

PAPER

Cycloaddition of alkynes to diimino Mo_3S_4 cubane-type clusters: a combined experimental and theoretical approach†

Cite this: DOI: 10.1039/c6nj01787h

Jose A. Pino-Chamorro,[a] Yuliya A. Laricheva,[b] Eva Guillamón,[c] María Jesús Fernández-Trujillo,[a] Emilio Bustelo,[a] Artem L. Gushchin,*[b] Nikita Y. Shmelev,[b] Pavel A. Abramov,[b] Maxim N. Sokolov,*[b] Rosa Llusar,*[c] Manuel G. Basallote*[a] and Andrés G. Algarra*[a]

Received (in Montpellier, France) 7th June 2016, Accepted 25th July 2016

DOI: 10.1039/c6nj01787h

www.rsc.org/njc

A heterocyclic ligand 4,4′-di-*tert*-butyl-2,2′-bipyridine (dbbpy) has been coordinated to the Mo_3S_4 cluster unit affording the complex $[Mo_3S_4Cl_3(dbbpy)_3]^+$ ($[\mathbf{1}]^+$) in a one-step ligand-exchange protocol from $[Mo_3S_4(tu)_8(H_2O)]Cl_4{\cdot}4H_2O$ (tu = thiourea). The new cluster was isolated as $[\mathbf{1}]PF_6$ and $[\mathbf{1}]Cl$ salts in high yields and the crystal structure of the latter determined by X-ray analysis. The synthetic procedure was extended to tungsten to afford $[W_3S_4Cl_3(dbbpy)_3]^+$ ($[\mathbf{2}]^+$). Kinetic and NMR studies show that $[\mathbf{1}]^+$ reacts with several alkynes to form dithiolene species *via* concerted [3+2] cycloaddition reactions whereas $[\mathbf{2}]^+$ remains inert under similar conditions. The different rates for the reactions of $[\mathbf{1}]^+$ are rationalised by computational (DFT) calculations, which show that the more electron-withdrawing the substituents of the alkyne the faster the reaction. The inertness of $[\mathbf{2}]^+$ is due to the endergonicity of its reactions, which feature ΔG_r values systematically 5–7 kcal mol^{-1} more positive than for those of $[\mathbf{1}]^+$.

1. Introduction

Molybdenum dithiolene complexes have been extensively studied since the 1960s due to their interesting properties and applications.[1] Broadly, compounds with five-membered $MoS_2C_2(R_2)$ chelate rings can be synthesised by reaction of a molybdenum compound with a preformed alkenedithiolate (or related species), *i.e.* Mo + $S_2C_2(R_2)$; or result from the addition of alkynes to molybdenum sulfides, *i.e.* MoS_2 + $C_2(R_2)$.[1a] The latter method, which implies the formation of two C–S bonds, has been used in the past to generate mono-,[2] di-,[3] and trinuclear[4–7] dithiolene complexes (see Scheme 1). Recently we became interested in the mechanistic aspects of the reaction between trinuclear $Mo_3(\mu\text{-}S)(\mu\text{-}S)_3$ species and alkynes (Scheme 1c), having

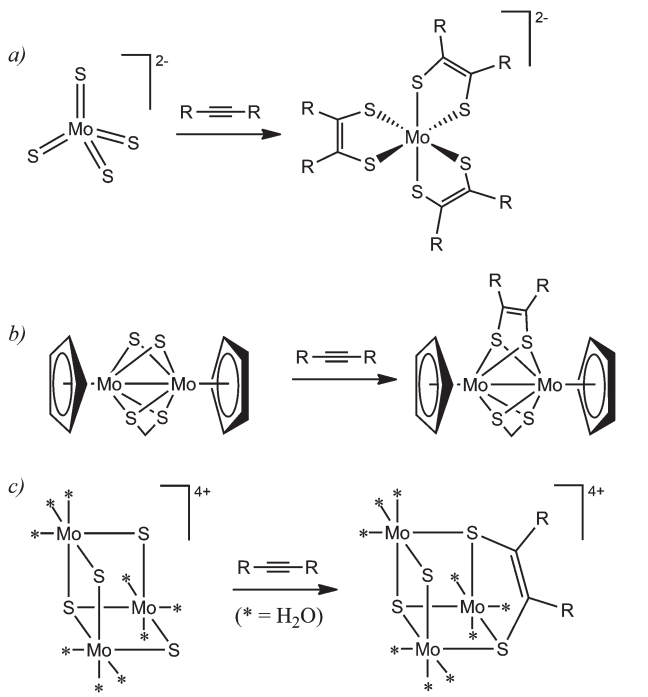

Scheme 1 Examples of mono- (a), di- (b), and trinuclear (c) molybdenum sulfides that react with alkynes leading to dithiolene complexes.

[a] Departamento de Ciencia de los Materiales e Ingeniería Metalúrgica y Química Inorgánica, Facultad de Ciencias, Instituto de Biomoléculas, Universidad de Cádiz, 11510 Puerto Real, Cádiz, Spain. E-mail: manuel.basallote@uca.es, andres.algarra@uca.es

[b] Nikolaev Institute of Inorganic Chemistry, Siberian Branch of the Russian Academy of Sciences and Novosibirsk State University, 630090 Novosibirsk, Russia. E-mail: gushchin@niic.nsc.ru

[c] Department de Química Física i Analítica, Universitat Jaume I, Av. Sos Baynat s/n, 12071 Castelló, Spain. E-mail: rosa.llusar@uji.es

† Electronic supplementary information (ESI) available: Results from kinetic, NMR and ESI-MS experiments, crystallographic data for [1]Cl·5H_2O, and Cartesian coordinates of all optimised structures. CCDC 1457770. For ESI and crystallographic data in CIF or other electronic format see DOI: 10.1039/c6nj01787h

analysed various factors that affect the kinetics and thermodynamics of the process from experimental and computational viewpoints.[8–10] Our results show that it can be viewed as a concerted [3+2] cycloaddition reaction between a $Mo(\mu\text{-}S)_2$ moiety of the cluster and the two carbon atoms of the alkyne; however, differences appear upon modification of the solvent, alkyne substituents, metal coordination environment, or the nature of the metal itself. For instance, while the $Mo_3S_4^{4+}$ aqua ion reacts with acetylene and other alkynes in a single kinetic step to produce the $[Mo_3(\mu_3\text{-}S)(\mu_2\text{-}S)(\mu_3\text{-}SCH{=}CHS)(H_2O)_9]^{4+}$ adduct or its analogues,[6,8] the $[Mo_3S_4(acac)_3(py)_3]^+$ (acac = acetylacetonate, py = pyridine) cluster shows a polyphasic kinetics which involves substitution of the pyridine ligands and further ligand reorganization.[9–10] Interestingly, no reaction is observed upon replacement of molybdenum by tungsten in the case of the acac-py cluster.[10] In contrast, the isothiocyanate tungsten complex $[W_3S_4(SCN)_9]^{5-}$ reacts with acetylene to afford a final product containing two acetylene groups with different coordination modes $[W_3(\mu_3\text{-}S)(\mu_3\text{-}SCH{=}CHS)(\mu\text{-}SCH{=}CH_2)(NCS)_9]^{5-}$.[5]

In order to shed more light on the mechanism of these processes, we decided to investigate the reaction of the trinuclear $[M_3S_4Cl_3(dbbpy)_3]^+$ complexes (M = Mo ($[\mathbf{1}]^+$) and W ($[\mathbf{2}]^+$)) with various alkynes. By doing so we are able to analyse the influence of the nature of the metal and the outer ligands in the cycloaddition process. $[\mathbf{1}]^+$ and $[\mathbf{2}]^+$ have been synthesised adapting a procedure recently published by some of us[11,12] on similar systems and the crystal structure of $[\mathbf{1}]^+$ has been determined by single-crystal X-ray diffraction methods. For the reaction of $[\mathbf{1}]^+$ and $[\mathbf{2}]^+$ with alkynes, unsaturated compounds with different substituents have been chosen. The reactions were investigated with stopped flow, spectroscopic and mass spectrometric techniques combined with mechanistic DFT studies.

2. Experimental

2.1. General remarks

Starting complexes $[Mo_3S_4(tu)_8(H_2O)]Cl_4{\cdot}4H_2O$ and $[W_3S_4(tu)_8(H_2O)]Cl_4{\cdot}2H_2O$ were prepared according to the published procedures.[11,12] All other reagents were obtained from commercial sources and used as received. Organic solvents were dried by standard methods before use.

2.2. Physical measurements

Elemental analyses were performed with a EuroEA3000 Eurovector analyser. IR spectra were recorded in the 4000–400 cm^{-1} range with a Perkin-Elmer System 2000 FTIR spectrometer with samples in KBr pellets. The characteristic IR frequencies for the bipyridine ligands were assigned on the basis of previous results. A triple quadrupole mass spectrometer with an orthogonal Z-spray electrospray source (Waters, Manchester) was used. The temperature of the source block was set to 100 °C, and the desolvation temperature was set to 120 °C. A capillary voltage of 3.3 kV was used in the positive scan mode, and the cone voltage was set to U_c = 20 V. Mass calibration from m/z = 50 to 3000 was performed with a solution of sodium iodide in 2-propanol/water (50 : 50). Sample solutions in CH_3CN were injected with a syringe pump directly connected to the ESI source at a flow rate of 10 μL min^{-1}. The observed isotopic pattern of each compound perfectly matched the theoretical isotope pattern calculated from their elemental composition by using the MassLynx 4.1 program.

2.2.1. Synthesis of $[Mo_3S_4Cl_3(dbbpy)_3][X]$ (X = Cl, PF_6). [**1**]Cl: a mixture of $[Mo_3S_4(tu)_8(H_2O)]Cl_4{\cdot}4H_2O$ (0.40 g, 0.32 mmol), 4,4′-di-*t*-butyl-2,2′-bipyridine (0.28 g, 1.0 mmol) and CH_3CN (40 mL) was refluxed for 5 hours. After cooling to room temperature, the resulting suspension was taken to dryness. The solid was then extracted with CH_2Cl_2, and the excess of insoluble thiourea was removed by filtration. The complex was precipitated with an excess of hexane to give a green-brown solid. Yield: 0.42 g (96%). For $C_{54}H_{72}N_6Cl_4Mo_3S_4$ (1363.08): calcd C 47.4; H 5.3, N 6.2; found C 47.0, H 5.6, N 5.9. ^{1}H NMR (500 MHz, 298 K, $CDCl_3$): δ 10.43 and 9.68 (d, dbbpy-$H^{2,2'}$, $^3J_{HH}$ = 6.1 Hz, 3H each); 8.46 and 8.22 (d, dbbpy-$H^{5,5'}$, $^4J_{HH}$ = 1.8 Hz, 3H each); 7.84 and 7.43 (dd, dbbpy-$H^{3,3'}$, $^3J_{HH}$ = 6.1 Hz, $^4J_{HH}$ = 2.0 Hz, 3H each); 1.60 and 1.46 (s, ^{t}Bu, 27H each). IR (KBr pellet): ν = 3096 (w), 2960 (vs), 2928 (s), 2868 (m), 1614 (vs), 1545 (m), 1483 (s), 1464 (m), 1410 (vs), 1366 (m), 1310 (w), 1295 (w), 1254 (m), 1204 (m), 1157 (w), 1128 (w), 1078 (w), 1024 (m), 899 (s), 837 (m), 727 (m), 644 (w), 606 (m), 550 (w), 484 (w), 457 (w) cm^{-1}. ESI-MS (+; CH_2Cl_2/CH_3CN, 50 : 50): m/z = 1327 $[M]^+$.

[**1**]PF_6: this compound was prepared by the same procedure than [**1**]Cl, but after removal of insoluble thiourea, the solution was loaded onto a silica gel column. After the column was washed with CH_2Cl_2, elution with a solution of KPF_6 in acetone (10 mg mL^{-1}) afforded a concentrated brown solution. This solution was evaporated to dryness, the residue extracted with CH_2Cl_2 and filtered in order to eliminate the inorganic salts. Finally the resulting solution was allowed to evaporate slowly in air to give 0.34 g (70%) of brown solid. For $C_{54}H_{72}N_6Cl_3F_6Mo_3PS_4$ (1472.60): calcd C 44.0; H 4.9, N 5.7; found C 44.3, H 5.1, N 5.6. ^{1}H NMR (500 MHz, 298 K, CD_2Cl_2): δ 10.35 and 9.51 (d, dbbpy-$H^{2,2'}$, $^3J_{HH}$ = 6.1 Hz, 3H each); 8.51 and 8.35 (d, dbbpy-$H^{5,5'}$, $^4J_{HH}$ = 1.8 Hz, 3H each); 7.76 and 7.42 (dd, dbbpy-$H^{3,3'}$, $^3J_{HH}$ = 6.1 Hz, $^4J_{HH}$ = 2.0 Hz, 3H each); 1.60 and 1.46 (s, ^{t}Bu, 27H each). IR (KBr pellet): ν = 3096 (w), 2965 (vs), 2873 (m), 1615 (vs), 1545 (m), 1484 (s), 1409 (vs), 1367 (m), 1253 (m), 1025 (m), 900 (m), 840 (vs), 558 (m) cm^{-1}. ESI-MS (+; CH_2Cl_2/CH_3CN, 50 : 50): m/z = 1327 $[M]^+$. UV/Vis (CH_3CN, see Fig. S1, ESI†): λ (ε) 650 nm (397 M^{-1} cm^{-1}).

2.2.2. Synthesis of $[W_3S_4Cl_3(dbbpy)_3][X]$. [**2**]Cl: this compound was prepared in a similar fashion to [**1**]Cl, but starting from a mixture of $[W_3S_4(tu)_8(H_2O)]Cl_4{\cdot}2H_2O$ (0.40 g, 0.27 mmol), 4,4′-di-*t*-butyl-2,2′-bipyridine (0.22 g, 0.82 mmol) and CH_3CN (40 mL), to give a green solid. Yield: 0.40 g (91%). For $C_{54}H_{72}N_6Cl_4W_3S_4$ (1626.77): calcd C 39.9; H 4.5, N 5.2; found C 39.5, H 4.3, N 5.5. ^{1}H NMR (500 MHz, 298 K, $CDCl_3$): δ 10.69 and 9.89 (d, dbbpy-$H^{2,2'}$, $^3J_{HH}$ = 6.1 Hz, 3H each); 8.72 and 8.48 (d, dbbpy-$H^{5,5'}$, $^4J_{HH}$ = 1.8 Hz, 3H each); 7.85 and 7.43 (dd, dbbpy-$H^{3,3'}$, $^3J_{HH}$ = 6.1 Hz, $^4J_{HH}$ = 2.0 Hz, 3H each); 1.54 and 1.40 (s, ^{t}Bu, 27H each). IR (KBr pellet): ν = 3093 (m., sh.), 2962 (s), 2876 (w), 1615 (vs), 1543 (m), 1483 (m), 1408 (vs), 1366 (m),

1306 (w), 1252 (m), 1203 (w), 1154 (w), 1126 (w), 1077 (w), 1023 (m), 930 (w), 900 (m), 841 (m), 740 (m), 607 (m), 553 (w), 468 (w) cm^{-1}. ESI-MS (+; CH_2Cl_2/CH_3CN, 50 : 50): m/z = 1591 $[M]^+$.

[**2**]PF_6: this compound was prepared in a way similar to the preparation of [**1**]PF_6 from [**1**]Cl, but starting from the tungsten cluster [**2**]Cl, to give 0.38 g (81%) of a green solid. $C_{54}H_{72}N_6Cl_3F_6W_3PS_4$ (1736.29): calcd C 37.4; H 4.2, N 4.9; found C 37.8, H 4.6, N 5.0. ^{1}H NMR (500 MHz, 298 K, CD_2Cl_2): δ 10.72 and 9.98 (d, dbbpy-H$^{2,2'}$, $^3J_{HH}$ = 6.1 Hz, 3H each); 8.48 and 8.25 (d, dbbpy-H$^{5,5'}$, $^4J_{HH}$ = 1.7 Hz, 3H each); 7.77 and 7.45 (dd, dbbpy-H$^{3,3'}$, $^3J_{HH}$ = 6.2 Hz, $^4J_{HH}$ = 1.8 Hz, 3H each); 1.57 and 1.42 (s, ^{t}Bu, 27H each). IR (KBr pellet): ν = 3099 (w), 2964 (s), 2873 (w), 1617 (vs), 1545 (w), 1484 (w), 1411 (s), 1368 (m), 1308 (w), 1253 (m), 1204 (w), 1129 (w), 1077 (w), 1029 (w), 902 (w), 841 (vs), 740 (w), 606 (w), 558 (s), 447 (w) cm^{-1}. ESI-MS (+; CH_2Cl_2/CH_3OH, 50 : 50): m/z = 1591 $[M]^+$. UV/Vis (CH_3CN): λ (ε) 600 nm (626 M^{-1} cm^{-1}).

2.3. Structural determination

Single crystals of [**1**]Cl·5H_2O suitable for X-ray analysis were obtained by recrystallization of [**1**]Cl from CH_2Cl_2/hexane mixture. The diffraction data were collected on a Super Nova, Dual (CuKα, λ = 1.5418 Å, at 200 K) by doing ϕ and ω scans of narrow (0.5°) frames. The structure was solved by direct methods and refined by full-matrix least-squares treatment against $|F|^2$ in anisotropic approximation with SHELXL program.[13] Absorption corrections were applied with SCALE3 ABSPACK scaling algorithm.[14] All non-hydrogen atoms were refined anisotropically. Hydrogen atoms of water molecules were not localised directly from the experiment. To observe all amounts of highly disordered water molecules a SQUEEZE procedure[15] and a PLATON program set[15] were used. This gives 150 e per unit cell or 2 additional water molecules per formula unit (in total 5 molecules per unit). Crystallographic data and refinement details are given in Table S1 (ESI†). CCDC 1457770.

2.4. Kinetic measurements

The kinetic experiments were carried out with an Applied Photophysics SX-18MV stopped-flow spectrometer provided with a PDA1 photodiode array detector, and with a Cary 50 Bio UV-Vis spectrophotometer. All experiments were carried out at 25.0 ± 0.1 °C in acetonitrile by mixing a solution of $[\mathbf{1}]^+$ (7.5×10^{-5} M) with another solution containing the alkyne in a concentration range large enough (0.01–0.50 M) to ensure pseudo-first order conditions. Preliminary experiments at two different cluster concentrations were carried out to confirm the first order dependence of the observed rate constants on this reagent. The spectral changes in the 700–1000 nm range were analysed with program SPECFIT-32.[17]

2.5. NMR experiments

NMR spectra were recorded on Agilent 500 and 600 DD2 and Bruker Avance 500 spectrometers at room temperature. Chemical shifts are given in parts per million from $SiMe_4$ (^{1}H and ^{13}C{^{1}H}) or $CFCl_3$ (^{19}F). ^{1}H and ^{13}C{^{1}H} NMR signal assignments were confirmed by ^{1}H-gCOSY, g-HSQC and g-HMBC experiments. NMR samples were prepared under Ar, although products are not particularly sensitive to air or humidity.

2.5.1. Isolation and NMR characterization of the type I product formed from $[\mathbf{1}]^+$ and dmad. 170 mg of cluster [**1**]PF_6 (0.115 mmol) were dissolved in 1 mL of CH_2Cl_2 under inert atmosphere, and 30 μL of the corresponding alkyne were added. The mixture was stirred for 15 min at room temperature. Then, 10 mL of Et_2O were added, causing the immediate precipitation of a dark brown solid, which was filtered, washed twice with Et_2O, and dried under vacuum, yielding 136 mg (73%).

[**1**]PF_6 + dmad: ^{1}H NMR (500 MHz, 298 K, CD_2Cl_2): δ 1.37–1.48 (s, 54H, C(C$\underline{H}_3$)$_3$), 3.41 and 3.53 (s, 3H each, COOC$\underline{H}_3$), 7.27–7.67 (br s, 6H, dbbpy-H$^{3,3'}$), 8.01–8.18 (br s, 6H, dbbpy-H$^{5,5'}$), 8.39, 10.04, 10.06, 10,42 and 10.61 (m, 6H, dbbpy-H$^{2,2'}$). ^{13}C{^{1}H} NMR (126 MHz, CD_2Cl_2): δ 30.47 (br s, C($\underline{C}$H$_3$)$_3$), 36.22 (br s, $\underline{C}$(CH$_3$)$_3$), 53.00 and 53.30 (s, COO$\underline{C}$H$_3$), 119.8–122.1 (s, dbbpy-C$^{5,5'}$), 123.0–125.5 (s, dbbpy-C$^{3,3'}$), 135.1 and 134.0 (s, S$\underline{C}$(COOCH$_3$)═$\underline{C}$(COOCH$_3$)S), 153.4–154.6 (s, dbbpy-C$^{6,6'}$), 154.3–159.7 (s, dbbpy-C$^{2,2'}$), 164.1 and 164.9 (s, $\underline{C}$OOCH$_3$), 165.8–168.9 (s, dbbpy-C$^{4,4'}$).

2.6. Computational details

DFT calculations were carried out with the Gaussian 09 (Revision D.01) suite of programs.[18] Geometry optimizations were carried out with the BP86 functional in combination with the SDD pseudopotentials and associated basis sets (BS1).[19] The clusters $[\mathbf{1}]^+$ and $[\mathbf{2}]^+$ were modelled using 2,2′-bipyridine instead of dbbpy ligands, *i.e.* as formally resulting from the substitution of ^{t}butyl groups by H atoms in the latter. Frequency calculations at the same level of theory confirmed that all the optimised structures on the potential energy surface correspond to either minima (all positive eigenvalues) or transition state structures (one imaginary eigenvalue). In addition, IRC calculations and subsequent geometry optimizations were employed confirmed the minima linked by each transition state.

All reported energies are free energies in solution, reported at 298.15 K and 1 atm. They are based on single-point gas phase energies with a larger basis set system, BS2, on the previously BS1-optimised structures, subsequently corrected by including thermal corrections from energy to free energy within the rigid-rotor-harmonic-oscillator, as well as single-point solvent and dispersion corrections. BS2 employs the SDD pseudopotentials and associated basis sets for Mo, W and S (with added d-orbital polarization on the latter[20]) and the Pople-style 6-311+G(2d,2p) basis set for the remaining atoms. Solvent corrections were computed at the BP86/BS1 level and made use of the PCM approach with standard parameters for acetonitrile.[21,22] Dispersion effects were included using Grimme's D3(BJ) parameter set.[23,24] Structures were generated using CYLview (color code: Mo (turquoise), W (blue), N (purple), Cl (green), S (yellow), C (grey), H (white)).[25]

3. Results and discussion

3.1. Synthesis and characterisation

In a previous work we have shown that the high lability of the thiourea ligands in easily accessible $[Mo_3S_4(tu)_8(H_2O)]Cl_4·4H_2O$

precursor can be used to prepare tri-substituted Mo_3S_4 complexes with 2,2′-bipyridine (bpy) and 1,10-phenanthroline(phen) ligands.[12] However, the resulting $[Mo_3S_4Cl_3(bpy)_3]Cl{\cdot}2H_2O$ and $[Mo_3S_4Cl_3(phen)_3]Cl{\cdot}4H_2O$ have low solubility in common organic solvents, even in DMF, which hinders their use for further transformations. In this work we have chosen 2,2′-bipyridine functionalised with *tert*-butyl groups in 4,4′-positions to solubilise the resulting Mo_3S_4 species. The desired $[Mo_3S_4Cl_3(dbbpy)_3]^+$ ($[\mathbf{1}]^+$) complex was obtained by reaction of $[Mo_3S_4(tu)_8(H_2O)]Cl_4{\cdot}4H_2O$ with dbbpy in CH_3CN and was isolated as air-stable [**1**]Cl and [**1**]PF_6 salts in 96% and 70% yields, respectively. In a similar manner the tungsten analogue $[\mathbf{2}]^+$ was synthesised from $[W_3S_4(tu)_8(H_2O)]Cl_4{\cdot}2H_2O$ and isolated as [**2**]Cl and [**2**]PF_6 salts in 91% and 81% yields, respectively.[11]

Single crystals of $[\mathbf{1}]Cl{\cdot}5H_2O$ were obtained by diffusion of hexane into a solution of [**1**]Cl in dichloromethane. The molecular structure of the $[Mo_3S_4Cl_3(dbbpy)_3]^+$ cation is shown in Fig. 1 together with a list of selected bond distances. The structure consists of an incomplete cuboidal arrangement in which the molybdenum and sulfur atoms occupy adjacent vertices with a missing metal position. Metal–metal and metal–sulfur distances within the Mo_3S_4 cluster core follow the same tendencies observed for other trinuclear Mo_3S_4 species.[26,27] Each molybdenum atom presents a distorted octahedral coordination environment, surrounded by three sulfur ligands, one chlorine, and the two nitrogen atoms of the dbbpy ligand. [**1**]$Cl{\cdot}5H_2O$ crystallises in *Pa*$\bar{3}$ space group due to the specific packing of the bulky cationic cluster units, which have almost spherical shape. Since $[Mo_3S_4Cl_3(phen)_3]Cl{\cdot}4H_2O$ crystallises in *P*3 group,[12] we believe that switching from 1,10-phenantroline (phen) to bulkier dbbpy ligands makes the cluster cations more spherical, so that they can be packed in a more symmetrical space group. The crystal structure of $[Mo_3S_4Cl_3(phen)_3]Cl{\cdot}4H_2O$ features weak C–H···Cl interactions that connect the cluster units into the sheets with 6^3 plane net topology, whereas in $[\mathbf{1}]Cl{\cdot}5H_2O$ the spherical form of the cluster cations prevents such interactions.

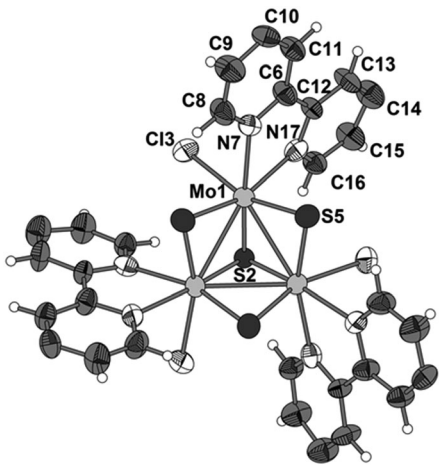

Fig. 1 ORTEP representation of $[Mo_3S_4Cl_3(dbbpy)_3]^+$ cation in [**1**]$Cl{\cdot}5H_2O$. *tert*-Bu groups are omitted for clarity. Average bond distances (Å): *d*(Mo–Mo) = 2.7680(11); *d*(Mo–μ_2-S) = 2.269(2), 2.298(2), *d*(Mo–μ_3-S) = 2.344(3); *d*(Mo–N) = 2.226(6), 2.245(7).

The structural integrity of $[\mathbf{1}]^+$ and $[\mathbf{2}]^+$ in solution has been proved by ^{1}H NMR spectroscopy and electrospray-ionization (ESI) mass spectrometry. The positive mass spectrum of $[\mathbf{1}]^+$ registered at 20 V shows the pseudomolecular peak centered at m/z = 1327 and a prominent peak at m/z = 665 attributed to the exchange of one chlorine atom by an acetonitrile solvent molecule $[\mathbf{1} - Cl + CH_3CN]^{2+}$ on the basis of the m/z value and its characteristic isotope pattern (see Fig. S2, ESI†). In the case of complex $[\mathbf{2}]^+$, the positive mass spectrum registered at 20 V only shows a signal corresponding with the pseudomolecular peak centered at m/z = 1591. ^{1}H NMR spectra for $[\mathbf{1}]^+$ and $[\mathbf{2}]^+$ shows that the symmetry found in the solid state is conserved in solution, featuring three equivalent dbbpy ligands asymmetrically bound to the metal centres. Therefore, six signals are observed for the dbbpy aromatic protons and two signals for the ^{t}Bu group protons.

3.2. Kinetic studies on the reaction of $[\mathbf{1}]^+$ and $[\mathbf{2}]^+$ with alkynes

In analogy with our previous studies on the reactivity of $[M_3S_4(acac)_3(py)_3]^+$ (M = Mo, W),[9,10] the reactions of $[\mathbf{1}]^+$ with a number of symmetrical and unsymmetrical alkynes were analysed. Specifically, the former group includes acetylene dicarboxylic acid (adc), dimethyl acetylenedicarboxylate (dmad) and 2-butyn-1,4-diol (btd), whereas phenylacetylene (PhA), propargyl alcohol (PrA) and ethylpropiolate (EtPr) belong to the latter. Spectral changes in the time scale of the stopped-flow technique are observed in all cases, with all reaction products showing an intense band centered at *ca.* 1000 nm and a shoulder at *ca.* 800 nm, as exemplified in Fig. 2 for the reaction with dmad. Unfortunately, the precise positions of the bands cannot be determined because they extend beyond the detector range. In any case, detailed analysis of the stopped-flow data indicates that a kinetic model with a single exponential is sufficient in all cases for a satisfactory fit, and therefore indicative of no subsequent processes. The appearance of the near-IR band is typical of [3+2] cycloaddition products of the

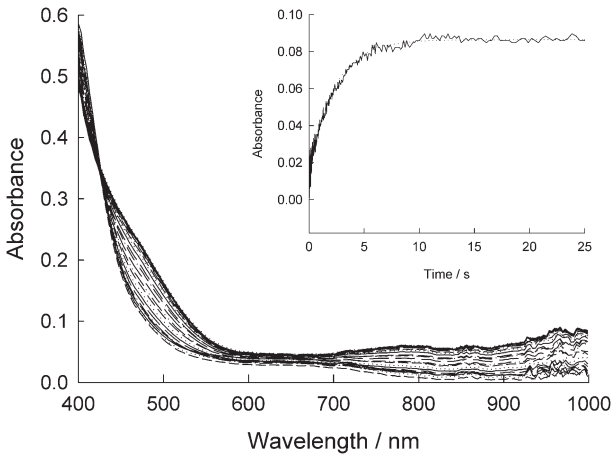

Fig. 2 Typical spectral changes for the reaction of [**1**]PF_6 with dmad in acetonitrile (T = 25.0 °C, [[**1**]PF_6] = 7.5 × 10^{-5} M, [dmad] = 0.017 M; time base = 100 seconds). Inset: Kinetic trace at 950 nm.

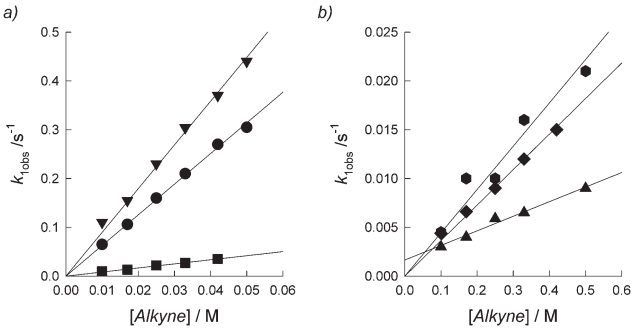

Fig. 3 Plot of the dependence of [alkyne] on the rate constants for the reaction of [**1**]PF_6 with: (a) dmad (▼), adc (●), EtPr (■); (b) PrA (⬣), PhA (◆), btd (▲) in acetonitrile solution at 25 °C.

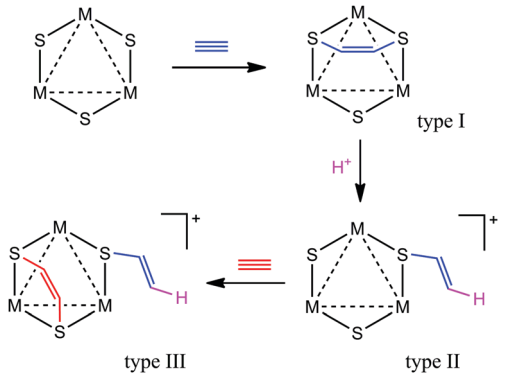

Scheme 2 Proposed mechanism for the formation of the so-called type I, II and III products between M_3S_4 (M = Mo, W) clusters and alkynes. For clarity the μ_3-S ligand and those completing the coordination environment of each M centre have not been included.

reaction between cuboidal clusters and alkynes,[5,6] so this spectral feature is indicative of double C–S bond formation. The effect of the metal centre (Mo *vs.* W) on the reaction with alkynes was tested by carrying out similar kinetic experiments with the tungsten compound $[\mathbf{2}]^+$. In spite of the variety of alkynes employed, no reaction was observed in the presence of any of them. This strongly resembles the results obtained for $[W_3S_4(acac)_3(py)_3]^+$, which reacted with neither of these alkynes.[10]

$$k_{1obs} = k_1 \cdot [\text{alkyne}] \quad (1)$$

$$k_{1obs} = k_1 \cdot [\text{alkyne}] + k_{-1} \quad (2)$$

The k_{1obs} values obtained for $[\mathbf{1}]^+$ under pseudo-first order conditions of alkyne excess show a linear dependence on the concentration of the latter (Fig. 3), and fitting to either eqn (1) or (2) leads to the second-order rate constants listed in Table 1. It is noteworthy that, for the reaction with btd, such linear dependence shows a nonzero intercept, indicative of a reversible process, and eqn (2) was employed accordingly. For comparison, Table 1 also includes a summary of the rate constants obtained for the first step of the reaction between $[Mo_3S_4(acac)_3(py)_3]^+$ and the same set of alkynes. In both cases it is clear that adc and dmad react faster than the remaining alkynes. This was rationalised as resulting from the different electron-withdrawing substituents of the alkyne.[9] All in all, the data in Table 1 indicate that modifications of the metal coordination sphere do not lead to substantial changes in the kinetics of reaction of these Mo clusters with a given alkyne.

Table 1 Summary of second order rate constants (M^{-1} s^{-1}) for the reaction of $[\mathbf{1}]^+$ and $[Mo_3S_4(acac)_3(py)_3]^+$ with an excess of alkyne in acetonitrile solution at 25 °C

Alkyne	$[\mathbf{1}]^+$	$[Mo_3S_4(acac)_3(py)_3]^+$ [a]
adc	6.3 ± 0.1	7.8 ± 0.2
dmad	9.0 ± 0.1	35 ± 1
EtPr	(8.4 ± 0.2) × 10^{-1}	—
PrA	(4.4 ± 0.2) × 10^{-2}	(3.74 ± 0.07) × 10^{-3} [c]
PhA	(3.64 ± 0.07) × 10^{-2}	(3.3 ± 0.1) × 10^{-3}
btd	(1.5 ± 0.2) × 10^{-2} [b]	(8.1 ± 0.1) × 10^{-3}

[a] From ref. 9 and 10. [b] Data fitted to eqn (2) with k_{-1} = (1.6 ± 0.3) × 10^{-3} s^{-1}. [c] Data fitted to eqn (2) with k_{-1} = (9 ± 1) × 10^{-5} s^{-1}.

An interesting experimental feature of the reaction between $[Mo_3S_4(acac)_3(py)_3]^+$ and alkynes consists in the appearance of subsequent kinetic steps for the formation of additional compounds beyond the so-called type I product formed in the initial [3+2] cycloaddition (Scheme 2). This behaviour has been observed for a number of other cuboidal clusters,[4,5,28] and Shibahara *et al.* proposed that such species are formed *via* protonation of the type I product,[5] which leads to the cleavage of one of the C–S bonds with formation of the so-called type II product, which again features a MS_2 unit available for the subsequent [3+2] cycloaddition of the second alkyne molecule, finally leading to the type III product. Dithiolate protonation is therefore required in this model to provide the MoS_2 unit necessary for a second cycloaddition. In order to test whether $[\mathbf{1}]^+$ can behave similarly, additional kinetic experiments for the reaction with dmad were carried out under an excess of trifluoroacetic acid.[29] Similar spectral changes were nonetheless observed, and in fact the overall fit of the whole set of data available led to a k_1 value of 9.8 ± 0.6 M^{-1} s^{-1}, analogous to that derived in the absence of the acid (see Fig. S3, ESI†). On the other hand, NMR experiments in the presence of, first an excess of dmad, and then an excess of trifluoroacetic acid, showed the release of the dbbpy ligands and, consequently, the cluster decomposition. When taken together with the stopped-flow information, these results suggest that dbbpy dissociation must occur in a slower time scale than the initial cycloaddition. Thus, protonation by strong acids leads to decomposition, whereas the reaction of $[\mathbf{1}]^+$ with alkynes in the presence of weaker carboxylic acids (such as adc) or without any acid stops after the formation of type I products. This behaviour is in contrast with that of $[Mo_3S_4(acac)_3(py)_3]^+$, which reacts with adc showing consecutive kinetic steps with participation of two alkyne molecules in addition to pyridine dissociation.[9]

Given that $[\mathbf{1}]^+$ and $[Mo_3S_4(acac)_3(py)_3]^+$ only differ in the ligands bound to the molybdenum centres, we believe that the results shown herein confirm our previously postulated hypothesis that the polyphasic kinetics of the reactions between

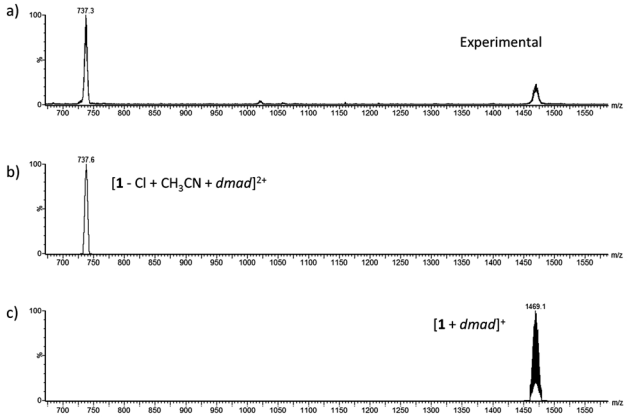

Fig. 4 ESI-MS spectrum of a solution 10^{-3} M of $[Mo_3S_4Cl_3(dbbpy)_3]^+$ in acetonitrile after addition of a 10 molar excess of dmad (a) together with the simulated spectra of $[\mathbf{1} - Cl + dmad + CH_3CN]^{2+}$ (b) and $[\mathbf{1} + dmad]^+$ (c).

$[Mo_3S_4(acac)_3(py)_3]^+$ and alkynes involve participation of the pyridine ligands.[9,10]

3.3. Product characterization by ESI-MS and NMR techniques

In order to confirm the nature of the cycloaddition product signaled by the appearance of the near IR band in the reaction products between $[\mathbf{1}]^+$ and alkynes, the reaction with dmad has been monitored by ESI-MS and NMR techniques. Mass spectrometry monitoring was performed by adding a ten molar excess of dmad to a 10^{-3} M cluster solution in acetonitrile (see Fig. 4). After ten minutes, the ESI spectrum of the reaction mixture shows a peak centered at m/z 1469 assigned to $[\mathbf{1} + dmad]^+$, *i.e.* the addition product of a single alkyne molecule, and a stronger peak centered at m/z 737, which results from the replacement of a chlorine atom by a solvent molecule, $[\mathbf{1} - Cl + dmad + CH_3CN]^{2+}$. Simulation of the isotopic distribution of these signals perfectly matches the experimental spectra. Notably, no relevant changes indicating addition of a second alkyne molecule are observed in the ESI-MS spectra of the reaction mixture at longer reaction times.

The reaction of $[\mathbf{1}]^+$ with an excess of dmad was also monitored by NMR in CD_2Cl_2. The ^1H NMR spectrum of the reaction product shows a large number of mostly overlapping and sometimes broad signals, accompanied by those corresponding to free dmad. Given that ESI-MS experiments rule out cluster decomposition, the resulting complex NMR pattern must be due to the lower symmetry of the resulting species, where dbbpy aromatic hydrogens become non-equivalent.

Bidimensional ^1H–^1H coupling experiments (gCOSY) allowed to elucidate the pattern showed by the aromatic signals. Based on the cross peaks with the neighbouring dbbpy-$H^{3,3'}$, it was possible to identify six resonances corresponding to dbbpy-$H^{2,2'}$. Hydrogens $H^{3,3'}$ and $H^{5,5'}$ show a reduced number of signals due to overlapping, but their overall peak integration also correspond to six. The formation of a dithiolene unit is supported by the presence of two singlet signals at 3.41 and 3.53 ppm corresponding to the carboxylate methyl groups, which become non-equivalent upon coordination to the

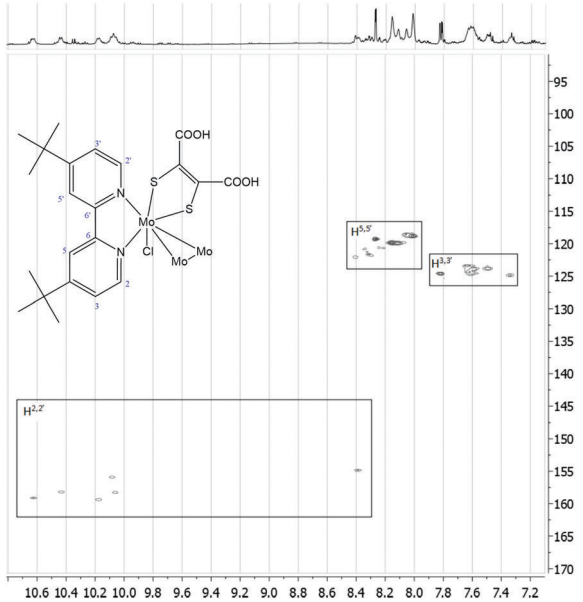

Fig. 5 Bidimensional HSQC spectrum of the species resulting from the reaction between $[\mathbf{1}]^+$ and dmad. Detail of the aromatic dbbpy ^1H–^{13}C cross-peaks.

cluster. The observed number of signals are attributable to the fully non-equivalent dbppy ligands (*i.e.* three ligands with two $H^{2,2'}$ atoms would give six resonances). $^{13}C\{^1H\}$ NMR assignment was performed with the help of two-dimensional HSQC and HMBC experiments. HSQC correlates directly bonded ^1H and ^{13}C nuclei and it allows to identify individually the twelve dbbpy-$C^{2,2'}$ resonances for the twelve dbbpy-$H^{2,2'}$ signals observed in the ^1H NMR spectra (see Fig. 5). Similarly, dbbpy-$C^{3,3'}$ and dbbpy-$C^{5,5'}$ were assigned. The dithiolene carbon atoms are both quaternary, and therefore they had to be identified from the $^{13}C\{^1H\}$ NMR spectrum by exclusion from HSQC. Note that they are the only carbons that show no correlations in this experiment. They appear at 135.1 and 134.0 ppm, values that compare well with those reported previously (133.1 and 136.7 ppm).[9,10] The remaining quaternary carbon atoms were identified by their HMBC long C–H correlation with neighboring protons. The carboxylate methyl groups in dmad adduct show a three-bond correlation with the carboxylic carbon atom, which appear at 164.1 and 164.9 ppm.

3.4. Computational (DFT) studies

The mechanism of formation of type I products between the clusters $[\mathbf{1}]^+$ and $[\mathbf{2}]^+$ and alkynes has been computationally analysed (see Computational details). The objective of the study is threefold: (a) to understand why $[\mathbf{2}]^+$ does not react with alkynes whereas $[\mathbf{1}]^+$ does; (b) to confirm that those reactions lead to type I products *via* concerted [3+2] cycloaddition processes, as has been described for other cuboidal clusters,[8–10] and (c), to analyse the effect of the substituents at the alkyne on the kinetics and thermodynamics of these cycloadditions. To do so, the reactions of the clusters $[\mathbf{1}]^+$ and $[\mathbf{2}]^+$ with all the alkynes employed in the experimental section were studied.

Table 2 Activation ($\Delta G^{\ddagger}$) and reaction (ΔG_r) free energies for the formation of type I reaction products between the clusters $[\mathbf{1}]^+$ and $[\mathbf{2}]^+$ with the studied alkynes (also including C_2H_2). The differences in these parameters, $\Delta\Delta G = \Delta G([\mathbf{2}]^+) - \Delta G([\mathbf{1}]^+)$, are also included. All values are given in kcal mol^{-1}

	$[\mathbf{1}]^+$		$[\mathbf{2}]^+$		Difference	
Alkyne	$\Delta G^{\ddagger}$	ΔG_r	$\Delta G^{\ddagger}$	ΔG_r	$\Delta\Delta G^{\ddagger}$	$\Delta\Delta G_r$
adc	6.0	−8.7	5.3	−3.3	−0.7	5.4
dmad	6.0	−9.1	5.8	−3.4	−0.2	5.7
Btd	12.1	−4.0	13.4	2.9	1.3	6.9
PrA	10.3	−5.5	12.5	2.1	2.2	7.6
PhA	8.4	−6.4	10.8	0.5	2.4	6.9
EtPr	7.5	−9.0	8.4	−1.8	1.5	7.2

The computations began with the optimization of the structures of the reactants, transition states, and corresponding type I reaction products for these reactions. Despite multiple attempts, in line with our previous mechanistic studies on the same reaction for other cuboidal clusters[8–10] it was only possible to locate transition states (TS) for the concerted formation of two C–S bonds between cluster and alkyne, *i.e.* no intermediates with one C–S bond were located. A summary of the activation ($\Delta G^{\ddagger}$) and reaction (ΔG_r) free energies for these concerted [3+2] cycloadditions is included in Table 2, whereas the structures of the computed TS and products for the reactions of both clusters with btd are depicted in Fig. 6 (see ESI† for Cartesian coordinates of all of them). The ΔG_r values in Table 2 clearly show that substitution of Mo by W leads to crucial changes in the thermodynamics of the processes, as the reaction free energies for $[\mathbf{2}]^+$ are systematically larger than those for $[\mathbf{1}]^+$ by 5–7 kcal mol^{-1}. This explains the experimentally observed lack of reaction between $[\mathbf{2}]^+$ and alkynes, as those thermodynamic differences make most of the reactions of this species endergonic while those of $[\mathbf{1}]^+$ are all exergonic. It is worth noting that small negative ΔG_r values are nonetheless obtained for the reactions of $[\mathbf{2}]^+$ with adc, dmad and EtPr, a discrepancy likely to be associated with the accuracy of the method. Regarding the free energy barriers, the values in Table 2 show that compared with $[\mathbf{1}]^+$, those of $[\mathbf{2}]^+$ are only 1–2 kcal mol^{-1} larger and thus still typical of reactions that take place relatively fast at room temperature. All in all, these results are similar to those reported for $[Mo_3S_4(acac)_3(py)_3]^+$ and its tungsten analogue,[10] where it was also concluded that the main effect of metal substitution consists of an increase in the reaction free energies. By using a combination of activation strain model and energy decomposition analyses that report showed that substituting Mo by W induces changes in the electronic structure of the cluster that result in weaker intra- and intermolecular orbital interactions. Interestingly, the smaller the distance between cluster and alkyne, the larger the energy difference between the potential energy surfaces for the reactions of both clusters with the same alkyne. Thus, as cluster and alkyne become closer throughout the [3+2] cycloaddition reaction, the differences in $\Delta G^{\ddagger}$ are always smaller than those in ΔG_r.[10]

In agreement with the similar ionic radii of molybdenum and tungsten,[30] substitution of Mo centers by W does not lead to significant geometrical changes. As exemplified in Fig. 6 for the reactions with btd, only small deviations in C–C and C–S bond distances are computed. Despite the concerted nature of the processes, confirmed by IRC calculations, analysis of the TS structures shows that in most cases one of the C–S bond forming distances is slightly longer than the other, *i.e.* for TS($[\mathbf{1}]^+$,btd) these are 2.43 and 2.53 Å. Similar differences in C–S bond distances at the TS structures for $[Mo_3S_4(acac)_3(py)_3]^+$ have been already reported, and these were explained on the basis of the different orientation of the R groups of RC≡CR alkynes, or the different steric and electronic properties of R and R′ groups in RC≡CR′ alkynes.[9] In the present case, such deviations are also expected to result from the coordination environment of the metal centres, which features two ligands with different *trans* effect, *i.e.* chloride and 2,2′-bipyridine, *trans* to the sulfur centres involved in the cycloaddition. This is supported by the computation of the hypothetical transition state for the reaction of $[\mathbf{1}]^+$ with acetylene, which yields C–S bond distances of 2.38 and 2.41 Å (see Fig. S4, ESI†).

From a kinetic point of view, the computed $\Delta G^{\ddagger}$ values for the reactions of $[\mathbf{1}]^+$ with alkynes are in line with the experimental rate constants, showing that those for the reactions with adc and dmad are slightly smaller than the remaining ones (see Table 2). Changing the substituents of the alkyne also leads to variations in the ΔG_r values, although in all cases product formation remains exergonic. In general, both kinetic and thermodynamic differences computed for the reactions of $[\mathbf{1}]^+$ with all the alkynes are similar to those reported for the reactions of $[Mo_3S_4(acac)_3(py)_3]^+$, and they can be explained

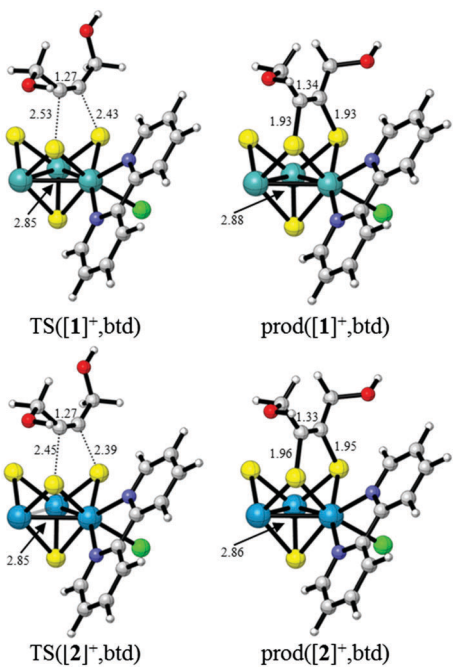

Fig. 6 DFT-optimised structures of the transition states and type I products of the [3+2] cycloaddition reaction between btd and the clusters $[\mathbf{1}]^+$ and $[\mathbf{2}]^+$. For clarity, only the dbbpy and chloride ligands bound to one metal centre are drawn. Selected distances are given in Å.

on the basis of the different electron-withdrawing properties of the substituents of the alkyne.[9]

4. Conclusions

New homoleptic diimino $M_3^{IV}S_4$ (M = Mo, W) clusters containing 4,4′-di-*tert*-butyl-2,2′-bipyridine (dbbpy) have been synthetised and fully characterised. The complexes were isolated as $[Mo_3S_4Cl_3(dbbpy)_3]X$ and $[W_3S_4Cl_3(dbbpy)_3]X$ (X = Cl, PF_6) salts in high yields. The crystal structure of $[Mo_3S_4Cl_3(dbbpy)_3]Cl\cdot 5H_2O$ has been determined by X-ray analysis. Similarly to other Mo_3S_4 incomplete cuboidal clusters,[6–10,28] $[\mathbf{1}]^+$ reacts with alkynes to form species bearing a bridging dithiolene unit *via* concerted [3+2] cycloaddition between the sp-hybridised carbon atoms of the alkyne and a $Mo(\mu\text{-}S)_2$ unit of the cluster. However, as observed for $[Mo_3S_4(acac)_3(py)_3]^+$, substitution of the molybdenum atoms of $[\mathbf{1}]^+$ by tungsten leads to a dramatic drop in reactivity, with the resulting tungsten cluster $[\mathbf{2}]^+$ unable to react with alkynes under similar experimental conditions.

Kinetic studies on the reactions between $[\mathbf{1}]^+$ and alkynes show that the rate of these processes depends on the employed alkyne, with adc and dmad reacting *ca.* two orders of magnitude faster than other alkynes. In contrast to $[Mo_3S_4(acac)_3(py)_3]^+$, $[\mathbf{1}]^+$ does not react further with alkynes after formation of type I cycloaddition products, thus indicating that the subsequent processes observed in the presence of $[Mo_3S_4(acac)_3(py)_3]^+$ are likely to involve the labile pyridine ligands.[9] The possibility of acid promoted formation of type II and III products between of $[\mathbf{1}]^+$ and dmad has been explored by carrying out experiments under excess of trifluoroacetic acid, however, no further reaction was observed. This contrasts with the reactivity reported for the water soluble clusters $[W_3(\mu_3\text{-}S)(\mu\text{-}O)(\mu\text{-}S)_2(NCS)_9]^{5-}$ and $[Mo_3(\mu_3\text{-}S)(\mu\text{-}S)_3(Hnta)_3]^{2-}$ (nta = 2,2′,2″-nitrilotriacetic acid), which have been shown to form type II cycloaddition products *via* protonation of the corresponding type I products in the presence of acid excess.[4,28] The results herein represent, on the one hand, an optimised procedure for the synthesis of the so-called type I cycloaddition products, with potential application for catalytic purposes; and on the other hand, they also provide a new starting point for the synthesis of type II and III products.

Computational (DFT) methods have been employed to get more insights into the mechanism of the reaction between alkynes and the clusters $[\mathbf{1}]^+$ and $[\mathbf{2}]^+$. The calculations confirm: (a) the concerted nature of the type I product formations, which take place *via* [3+2] cycloaddition processes; (b) the marked effect of the substituents of the alkyne on the kinetics of the reactions of $[\mathbf{1}]^+$: the more electron-withdrawing the substituent the faster the reaction;[9] and (c), that the lack of reaction between $[\mathbf{2}]^+$ and alkynes has a thermodynamic origin, as for $[\mathbf{2}]^+$ reaction free energies are systematically *ca.* 5–7 kcal mol^{-1} more positive than for $[\mathbf{1}]^+$, and this leads to endergonic processes.[10]

Acknowledgements

Financial support of the Russian Foundation for Basic Research (grant 15-03-02775) is gratefully acknowledged. Financial support of the Spanish Ministerio de Economia y Competitividad and FEDER funds from the European Union (grants CTQ2015-65707-C2-2-P and CTQ2015-65207-P), Universitat Jaume I (research project P1.1B2013-40) and Generalitat Valenciana (PrometeoII/2014/022) is gratefully acknowledged. The authors are also grateful to the SCIC of the Universitat Jaume I for providing mass spectrometry facilities and the University of Cádiz for computing resources.

Notes and references

1 (*a*) E. I. Stiefel, *Dithiolene Chemistry: Synthesis, Properties, and Applications*, Wiley, 2004, vol. 52; (*b*) , *Coord. Chem. Rev.*, 2010, **254**, 1357–1588.
2 D. Coucouvanis, A. Hadjikyriacou, A. Toupadakis, S. M. Koo, O. Ileperuma, M. Draganjac and A. Salifoglou, *Inorg. Chem.*, 1991, **30**, 754–767.
3 M. McKenna, L. L. Wright, D. J. Miller, L. Tanner, R. C. Haltiwanger and M. R. DuBois, *J. Am. Chem. Soc.*, 1983, **105**, 5329–5337.
4 M. Maeyama, G. Sakane, R. Pierattelli, I. Bertini and T. Shibahara, *Inorg. Chem.*, 2001, **40**, 2111–2119.
5 Y. Ide, M. Sasaki, M. Maeyama and T. Shibahara, *Inorg. Chem.*, 2004, **43**, 602–612.
6 T. Shibahara, G. Sakane and S. Mochida, *J. Am. Chem. Soc.*, 1993, **115**, 10408–10409.
7 (*a*) Y. Ide and T. Shibahara, *Inorg. Chem. Commun.*, 2004, **7**, 1132–1134; (*b*) Y. Ide and T. Shibahara, *Inorg. Chem.*, 2007, **46**, 357–359; (*c*) T. Shibahara, K. Kawamoto, A. Matsuura, H. Takagi, T. Nishioka, I. Kinoshita and H. Akashi, *Bull. Chem. Soc. Jpn.*, 2014, **87**, 459–469.
8 J. Á. Pino-Chamorro, A. G. Algarra, M. J. Fernández-Trujillo, R. Hernández-Molina and M. G. Basallote, *Inorg. Chem.*, 2013, **52**, 14334–14342.
9 J. Á. Pino-Chamorro, A. L. Gushchin, M. J. Fernández-Trujillo, R. Hernández-Molina, C. Vicent, A. G. Algarra and M. G. Basallote, *Chem. – Eur. J.*, 2015, **21**, 2835–2844.
10 E. Bustelo, A. L. Gushchin, M. J. Fernández-Trujillo, M. G. Basallote and A. G. Algarra, *Chem. – Eur. J.*, 2015, **21**, 14823–14833.
11 Y. A. Laricheva, A. L. Gushchin, P. A. Abramov and M. N. Sokolov, *J. Struct. Chem.*, 2016, **57**, 1000–1007.
12 A. L. Gushchin, Y. A. Laricheva, P. A. Abramov, A. V. Virovets, C. Vicent, M. N. Sokolov and R. Llusar, *Eur. J. Inorg. Chem.*, 2014, 4093–4100.
13 C. B. Hubschle, G. M. Sheldrick and B. Dittrich, *J. Appl. Crystallogr.*, 2011, **44**, 1281–1284.
14 CrysAlis PRO, Agilent Technologies, Version 1.171.36.28, release 01–02–2013 CrysAlis171.NET.
15 P. van der Sluis and A. L. Spek, *Acta Crystallogr., Sect. A: Found. Crystallogr.*, 1990, **46**, 194–201.
16 A. Spek, *Acta Crystallogr., Sect. D: Biol. Crystallogr.*, 2009, **65**, 148–155.
17 R. A. Binstead, B. Jung and A. D. Zuberbühler, *SPECFIT-32*, Spectrum Software Associates, Chappel Hill, 2000.

18 M. J. Frisch, G. W. Trucks, H. B. Schlegel, G. E. Scuseria, M. A. Robb, J. R. Cheeseman, G. Scalmani, V. Barone, B. Mennucci, G. A. Petersson, H. Nakatsuji, M. Caricato, X. Li, H. P. Hratchian, A. F. Izmaylov, J. Bloino, G. Zheng, J. L. Sonnenberg, M. Hada, M. Ehara, K. Toyota, R. Fukuda, J. Hasegawa, M. Ishida, T. Nakajima, Y. Honda, O. Kitao, H. Nakai, T. Vreven, J. A. Montgomery, Jr., J. E. Peralta, F. Ogliaro, M. Bearpark, J. J. Heyd, E. Brothers, K. N. Kudin, V. N. Staroverov, T. Keith, R. Kobayashi, J. Normand, K. Raghavachari, A. Rendell, J. C. Burant, S. S. Iyengar, J. Tomasi, M. Cossi, N. Rega, J. M. Millam, M. Klene, J. E. Knox, J. B. Cross, V. Bakken, C. Adamo, J. Jaramillo, R. Gomperts, R. E. Stratmann, O. Yazyev, A. J. Austin, R. Cammi, C. Pomelli, J. W. Ochterski, R. L. Martin, K. Morokuma, V. G. Zakrzewski, G. A. Voth, P. Salvador, J. J. Dannenberg, S. Dapprich, A. D. Daniels, O. Farkas, J. B. Foresman, J. V. Ortiz, J. Cioslowski and D. J. Fox, *Gaussian 09, Revision D.01*, Gaussian, Inc., Wallingford, CT, 2013.

19 D. Andrae, U. Haussermann, M. Dolg, H. Stoll and H. Preuss, *Theor. Chim. Acta*, 1990, **77**, 123–141.

20 A. Hollwarth, M. Bohme, S. Dapprich, A. W. Ehlers, A. Gobbi, V. Jonas, K. F. Kohler, R. Stegmann, A. Veldkamp and G. Frenking, *Chem. Phys. Lett.*, 1993, **208**, 237–240.

21 M. Cossi, G. Scalmani, N. Rega and V. Barone, *J. Chem. Phys.*, 2002, **117**, 43–54.

22 J. Tomasi, B. Mennucci and R. Cammi, *Chem. Rev.*, 2005, **105**, 2999–3093.

23 S. Grimme, J. Antony, S. Ehrlich and H. Krieg, *J. Chem. Phys.*, 2010, **132**, 154104.

24 S. Grimme, S. Ehrlich and L. Goerigk, *J. Comput. Chem.*, 2011, **32**, 1456–1465.

25 C. Y. Legault, CYLview, 1.0b, Université de Sherbrooke, Canada, 2009, http://www.cylview.org.

26 A. G. Algarra, M. G. Basallote, M. J. Fernández-Trujillo, M. Feliz, E. Guillamón, R. Llusar, I. Sorribes and C. Vicent, *Inorg. Chem.*, 2010, **49**, 5935–5942.

27 A. G. Algarra, M. G. Basallote, M. J. Fernández-Trujillo, E. Guillamón, R. Llusar, M. D. Segarra and C. Vicent, *Inorg. Chem.*, 2007, **46**, 7668–7677.

28 H. Takagi, Y. Ide and T. Shibahara, *C. R. Chim.*, 2005, **8**, 985–992.

29 Note that adc features two carboxylic acid groups that could facilitate such subsequent processes. However, in acetonitrile solution these should be weak and therefore not readily deprotonated. See: K. Izutsu, *Acid-Base Dissociation Constants in Dipolar Aprotic Solvents*, IUPAC Chemical Data Series, Blackwell, Oxford, 1990, vol. 35.

30 G. R. Chhatwal and H. Mehra, in *Advanced Inorganic Chemistry*, ed. G. Pub, Krishna Prakashan, 1974, vol. 1.